

Superconductivity in monoclinic TiO film

Shihao Liu(刘仕豪), Zongyao Huang(黄宗耀), Huiyu Wang(王慧宇), Wei Hu(胡卫), Xiangyu Hua(华翔宇), Zhaohang Li(李朝航), Zhiwei Wang(王智炜), Feixiong Quan(全飞熊), Zhen Wang(王臻), Jing Tao(陶靖), Tao Wu(吴涛), Xigang Luo(罗习刚), and Xianhui Chen(陈仙辉)

Citation: Chin. Phys. B, 2026, 35 (**7**): 077403. DOI: 10.1088/1674-1056/ae6b3d
http://cpb.iphy.ac.cn; http://iopscience.iop.org/cpb

What follows is a list of articles you may be interested in

Vortex matching effects and flux dynamics manipulation in MgB_2 thin films via He-FIB-induced periodic artificial pinning centers

Ying Han(韩颖), Dali Yin (殷大利), Xinwei Cai(蔡欣炜), Yan Zhang(张焱), Yue Wang(王越), Lifeng Tian(田利丰), and Zizhao Gan(甘子钊)

Chin. Phys. B, 2026, 35 (**6**): 067405. DOI: 10.1088/1674-1056/ae3c8d

Emergent topological superconductivity in skyrmion magnet/d-wave superconductor heterostructures

Zhi-Jian Li(李志坚) and Qiang Han(韩强)

Chin. Phys. B, 2026, 35 (**6**): 067403. DOI: 10.1088/1674-1056/ae4c6e

From stacking to function: Emergent states and quantum devices in 2D superconductor heterostructures

Sichun Zhao(赵思莼), Junlin Xiong(熊俊林), Ji Zhou(周吉), Shi-Jun Liang(梁世军), Bin Cheng(程斌), and Feng Miao(缪峰)

Chin. Phys. B, 2026, 35 (**6**): 067402. DOI: 10.1088/1674-1056/ae4c6c

Superconductivity in bulk 2H-MoS_2 via carrier doping

Mingshu Tan(谭明蜀), Helin Mei(梅贺林), Keyi Li(李可意), Wei Ren(任玮), Xueying Ma(马雪英), Shaoshuai Hou(侯少帅), Feng Jin(金峰), Anmin Zhang(张安民), and Qingming Zhang(张清明)

Chin. Phys. B, 2026, 35 (**5**): 057403. DOI: 10.1088/1674-1056/ae3c93

Manipulating the electronic structure and superconductivity of Li_2B_3C by biaxial strain

Yuhao Gu(顾雨豪), Yihao Wang(王奕淏), and Shuxian Hu(胡淑贤)

Chin. Phys. B, 2026, 35 (**4**): 047401. DOI: 10.1088/1674-1056/ae5594

RAPID COMMUNICATION

Superconductivity in monoclinic TiO film

Shihao Liu(刘仕豪)[1,†], Zongyao Huang(黄宗耀)[1,†], Huiyu Wang(王慧宇)[1], Wei Hu(胡卫)[2], Xiangyu Hua(华翔宇)[1], Zhaohang Li(李朝航)[1], Zhiwei Wang(王智炜)[1], Feixiong Quan(全飞熊)[1], Zhen Wang(王臻)[1], Jing Tao(陶靖)[1], Tao Wu(吴涛)[1], Xigang Luo(罗习刚)[1], and Xianhui Chen(陈仙辉)[1,3,4,‡]

[1] *Department of Physics, University of Science and Technology of China, Hefei* 230026, *China*
[2] *Institute of Physics, Chinese Academy of Sciences, Beijing* 101499, *China*
[3] *CAS Center for Excellence in Superconducting Electronics (CENSE), Shanghai* 200050, *China*
[4] *CAS Center for Excellence in Quantum Information and Quantum Physics, Hefei* 230026, *China*

(Received 3 April 2026; revised manuscript received 4 May 2026; accepted manuscript online 11 May 2026)

Titanium oxide films garner substantial research attention among binary oxides since the superconducting transition temperature of cubic TiO significantly rises from around 2 K in bulk to 7.4 K in thin films. In this study, titanium oxide thin films were fabricated using magnetron sputtering on Al_2O_3 substrates, where spatially multiphase coexistence was observed. By incorporating a Gd-doped CeO_2 (GCO) buffer layer, we achieved the epitaxial growth of single-phase monoclinic TiO thin films, which exhibit a superconducting transition temperature of 5 K. Concurrently, a previously unreported superstructure is identified within the GCO intermediate layer, arising from oxygen vacancy ordering during heteroepitaxial growth. These findings confirm the emergence of superconductivity in the monoclinic titanium oxide system and provide valuable insights into elucidating the relationship between the structures and properties of various titanium oxides, as well as the ion redistribution mechanisms during the synthesis of complex oxide thin films.

Keywords: superconductivity, titanium oxide, thin film, cerium dioxide, superlattice, polaron

PACS: 74.25.–q, 74.25.F–, 74.78.–w, 01.50.ff

DOI: 10.1088/1674-1056/ae6b3d **CSTR:** 32038.14.CPB.ae6b3d

1. Introduction

The physicochemical properties of materials are intrinsically governed by structural configurations, and systematic investigation of structure–property correlations provides fundamental insights for advancing functional material design.[1–3] Especially for the vast oxide family, diverse crystal structures and stoichiometric ratios generate rich physical properties. For instance, in cuprate and nickelate high-temperature superconductors, variations in crystal structures and oxygen content can significantly influence their superconducting transition temperatures.[4–9] Within the extensive family of functional oxides, titanium oxides, represented by titanium dioxide, have garnered significant attention owing to their remarkable, versatile optoelectronic characteristics.[10–13] Moreover, following the successful fabrication of cubic TiO thin films with a superconducting transition temperature of 7.4 K ($\sim$ 2 K for the bulk material), the growth of superconducting titanium oxide films with distinct structures has drawn increasing attention.[14–16] However, titanium oxides possess complex and diverse structures. Comprehensive characterization of the film structures and reliable measurements of the intrinsic physical properties of single-phase samples are still lacking, and the structure–property correlation across different samples has also been rarely reported.

Subsequent investigations have identified a series of superconducting titanium oxide films, including Ti_2O_3 ($T_c \approx$ 8.0 K),[17] Ti_3O_5 ($T_c \approx$ 7.1 K), Ti_4O_7 ($T_c \approx$ 3.0 K),[18] and Mg:Ti_9O_{10} ($T_c \approx$ 5.0 K) [19] systems. Despite their diverse structures, titanium oxide thin films commonly show multiphase coexistence during growth, driven by varying growth conditions and thickness.[20] Such multiphase states are difficult to distinguish using a single structural characterization technique, leading to severe challenges in the study of intrinsic physical properties and further underscoring the importance of growing single-phase thin films. In general, the main strategies for growing single-phase films include selecting appropriate substrates and orientations, precisely controlling growth conditions (e.g., temperature, atmosphere, growth rate, etc.), applying suitable annealing treatments, and depositing buffer layers.[21–25] Notably, as widely employed buffer layer materials, GCO confers distinct advantages in oxide heteroepitaxy, particularly for cuprate high-T_c superconductors. The exceptional oxygen diffusivity at elevated thermal regimes may underpin observed interfacial enhancement effects.[26–28] Owing to its high ionic conductivity, GCO interlayer also functions as an effective solid-state oxygen-ion transport medium and can

[†] These authors contributed equally to this work.

[‡] Corresponding author. E-mail: chenxh@ustc.edu.cn

© 2026 Chinese Physical Society and IOP Publishing Ltd. All rights, including for text and data mining, AI training, and similar technologies, are reserved.

regulate the oxygen content in oxides. This capability has been validated in diverse systems, including $Bi_2Sr_2CaCu_2O_{8+\delta}$ ultrathin crystallites and $SrCoO_{2.5}$ epitaxial layers.[29,30] Meanwhile, relying on its unique oxygen vacancies and oxygen transport capabilities, cerium dioxide has also emerged as a catalytic material that has drawn significant attention, demonstrating excellent performance.[31,32] Systematic interrogation of GCO-mediated crystallization kinetics could elucidate fundamental mechanisms governing these structure-property relationships.

In this work, we successfully synthesized a vacancy-ordered monoclinic TiO film utilizing a GCO buffer layer, demonstrating superconducting transition at 5 K, and through the analysis of the transport behavior, we conclude that polarons play a significant role in titanium oxide films. Moreover, we conducted a detailed analysis of the structure of m-TiO and the related c-TiO, and confirmed it through multiple structural characterization methods. This introduces a new member to the series of superconducting titanium oxide films and provides a reference for systematically elucidating the relationship between their properties and structural evolution. In addition, the growth selectivity on different substrates or buffer layers also provides a reference for the connection between different titanium oxide structures. In our experimental configuration, the implementation of a GCO intermediate layer during oxide film deposition resulted in spontaneous superstructure formation. This phenomenon provides compelling evidence for the critical role of oxygen anion migration pathways and vacancy self-organization processes in determining crystallographic evolution during heteroepitaxial growth processes.

2. Experimental details

The GCO ($Ce_{0.8}Gd_{0.2}O_{1.9+x}$) film was deposited on (00l)-oriented $SrTiO_3$ (STO) substrate using radio-frequency (RF) magnetron sputtering with a 3-inch sintered 20% Gd-doped CeO_2 ceramics target (99.9% purity). The ceramic target was fabricated via the sol–gel technique prior to sputtering. The deposition chamber was evacuated to a base pressure better than 1×10^{-6} Torr before growth. During deposition, the RF power was maintained at 65 W with a gas mixture of Ar/O_2 (3:1 flow ratio) at a total pressure of 20 mTorr. Substrate temperature was stabilized at 700 °C. The sputtering system featured a rotating substrate holder positioned 130 mm above the target, yielding compositionally uniform 500-nm-thick films. Post-deposition, films underwent *in situ* annealing at 700 °C for 2 hours in a 50 mTorr O_2 atmosphere. The temperature was subsequently ramped to the optimal condition for immediate growth of the subsequent TiO layer.

The TiO film was deposited on (00l)-oriented GCO film and Al_2O_3(0001) substrate by RF magnetron sputtering using a 3-inch sintered ceramic target with 99.9% purity. During deposition, the RF power energy, growth temperature, and pressure of pure argon were fixed at 60 W, 850 °C, and 20 mTorr, respectively. The thickness of the TiO films used for subsequent characterizations is about 80 nm, with a growth rate of 15 nm/h. After deposition, the films were cooled to room temperature under high-vacuum conditions ($< 1\times10^{-6}$ Torr). X-ray diffraction (XRD) data were collected by an x-ray diffractometer (SmartLab-9, Rigaku Corp.) with Cu K_α radiation. The electrical and magnetic transport properties were measured by the physical property measurement system (PPMS). The magnetization measurements were performed with the vibrating sample magnetometer (VSM). High-resolution transmission electron microscopy (HRTEM) images were obtained on a Thermo Scientific Themis Z microscope equipped with a probe-forming spherical aberration corrector.

850 °C is determined as the optimal growth temperature, at which the resulting samples exhibit the highest superconducting transition temperature. 900 °C corresponds to the upper temperature limit of the experimental apparatus. Samples fabricated at 775 °C and above exhibit good experimental reproducibility, while a further reduction in growth temperature leads to a pronounced deterioration of phase formation. The selection of other experimental parameters is also based on the criterion of obtaining optimal sample quality. No oxygen is introduced during TiO growth. Even the minimum oxygen flow rate permitted by the instrument will cause complete oxidation of titanium, which hinders the formation of the desired phase.

3. Results

3.1. Structural description and characterization of the titanium monoxide thin films.

Figure 1(a) presents a schematic of the monoclinic TiO (m-TiO) crystal structure. From a structural perspective, the monoclinic TiO (m-TiO) phase displays a vacancy-ordered configuration that is distinct from the conventional cubic TiO (c-TiO) phase. To illustrate this, we compared the (001) surfaces of c-TiO and m-TiO. Figure 1(d) shows the crystal structure of c-TiO on the left, while the right side presents a schematic diagram depicting the distribution of titanium and oxygen atoms within the (001) plane. Additionally, Fig. 1(e) illustrates the atomic distribution and vacancy arrangement within the (001) plane of m-TiO. By comparing the atomic distributions within the ab-plane in Figs. 1(d) and 1(e), we reveal the regular vacancy arrangement: along the positive 45° diagonal direction, every two columns of oxygen or titanium chains are accompanied by a column of defect chains, in which half of the oxygen or titanium atoms are periodically missing at regular intervals. The defective oxygen and titanium chains alternate in this arrangement. This comparison confirms structural similarity between the two phases.

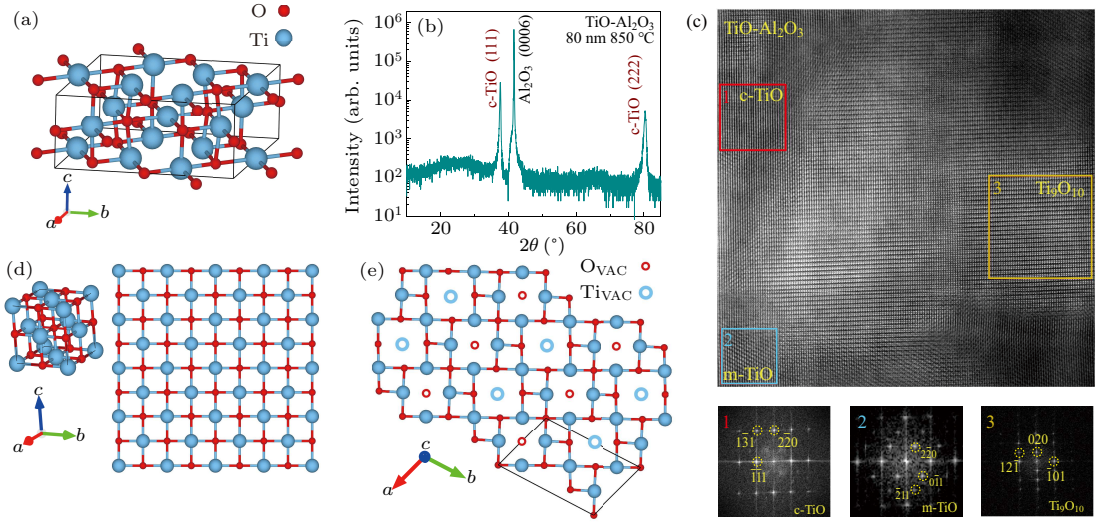


Fig. 1. (a) Schematic of the monoclinic m-TiO unit cell. (b) Out-of-plane XRD θ–2θ scan spectra for TiO film grown on Al_2O_3(0001) substrate. (c) HRTEM images of titanium oxide films grown on an Al_2O_3(0001) substrate. Three structures encompass the c-TiO phase, the m-TiO phase, and an orthorhombic Ti_9O_{10} phase coexist in film space, which are distinguished by red, blue, and yellow, respectively. The corresponding FFT patterns along the [112], [101] and $[\bar{1}\bar{1}\bar{1}]$ directions are presented in the lower three panels. (d) Schematic diagram of cubic-phase TiO crystal on the left side and diagram within the (001) plane on the right. (e) Schematic of the (001) plane of monoclinic TiO. Oxygen vacancies and titanium vacancies are respectively indicated by red and blue circles, which can be directly observed by comparing the atomic distributions in panels (d) and (e).

Due to the variable oxidation states of titanium and the close structural relationship among titanium oxide compounds, thin films of different oxidation states often exhibit phase coexistence. Several studies have highlighted this phenomenon, making the fabrication of single-phase titanium oxide films a significant challenge.[20] This observation is also evident in our experiments. As shown in Fig. 1(b), the x-ray diffraction (XRD) pattern of TiO thin films directly grown on Al_2O_3(0001) substrates is consistent with previous reports, displaying a (111) diffraction peak characteristic of the c-TiO phase.[15] However, further electron microscopy results reveal the presence of three distinct oxidation states in different regions of the sample, as shown in Fig. 1(c). These states include 1) cubic phase, 2) monoclinic phase, and 3) orthorhombic Ti_9O_{10}, which are distinguished by red, blue, and yellow, respectively. The corresponding fast Fourier transform (FFT) images (shown in the lower three panels of Fig. 1(c)) further confirm these findings. This suggests that there are certain structural similarities between different TiO phases, leading to a common coexistence. Moreover, this indicates that a single structural characterization technique, such as XRD, is insufficient for accurately distinguishing between these phases.

To obtain a single-phase titanium oxide thin film, and considering the potential modulation of the film's structure and properties due to epitaxial strain, we also attempted to grow the titanium oxide on $SrTiO_3$ substrates and STO substrates with a GCO buffer layer. Figure 2(b) presents the x-ray diffraction (XRD) pattern of the titanium oxide film grown on a STO substrate. The diffraction peak around 42° may correspond to the (200) diffraction peak of cubic TiO, and similar results are observed on $(La_{0.3}Sr_{0.7})(Al_{0.65}Ta_{0.35})O_3$ (LSAT) substrates (see supplementary materials, Fig. S1). However, this diffraction peak appears in multiple TiO phases, such as Ti_4O_7 and Ti_9O_{10}, and, as seen with the Al_2O_3 substrate, it cannot be used to distinctly identify the specific structure. Subsequently, we attempted to grow TiO thin films by first depositing a GCO buffer layer. Figure 2(a) shows the XRD pattern for the monoclinic TiO film epitaxially grown on a (00l)-oriented $SrTiO_3$ substrate with a (00l)-oriented GCO buffer layer, revealing distinct diffraction peaks corresponding to monoclinic TiO, GCO, and the substrate. In contrast to the previous results without a buffer layer, the diffraction peak around 42° no longer appears; instead, a set of diffraction peaks corresponding to the m-TiO phase emerges, indicating the formation of a pure monoclinic phase.

Given the complexity of the titanium oxide system, employing multiple characterization techniques is essential. Figure 2(c) shows the reciprocal space map (RSM) of monoclinic TiO(002)/GCO(002)/STO(001) taken along the [100] substrate direction. In addition to the peaks corresponding to the $SrTiO_3$ substrate, GCO film, and monoclinic TiO, a new set of regular diffraction peaks, marked with asterisks, is observed. These peaks are attributed to a new superlattice formed by oxygen vacancies in the GCO buffer layer. The difference between c-TiO in the [001] direction and m-TiO in the $[1\bar{1}1]$ direction is illustrated in the inset of Fig. 2(c). The identification of m-TiO$(1\bar{1}3)$ and m-TiO$(1\bar{1}1)$ reflections along the $[1\bar{1}0]$ zone axis unambiguously distinguishes the monoclinic phase from the cubic TiO along the [001] direction, confirming the single-phase monoclinic TiO in our sample.

To further confirm the cross-sectional structure of the m-TiO film epitaxially grown on the cubic GCO buffer layer, we performed additional electron microscopy characterizations. HRTEM images shown in Figs. 3(a) and 3(b) reveal two rep-

resentative grains oriented along the $[\bar{1}\bar{1}\bar{1}]$ and [111] directions relative to the incident electron beam. The lattice images and corresponding FFT analyses across the film (insets of Figs. 3(a) and 3(b)) confirm the exclusive presence of the m-TiO phase, with no other TiO phases observed. These structural characterization results collectively demonstrate that the growth of the GCO buffer layer enables the formation of a single-phase TiO film.

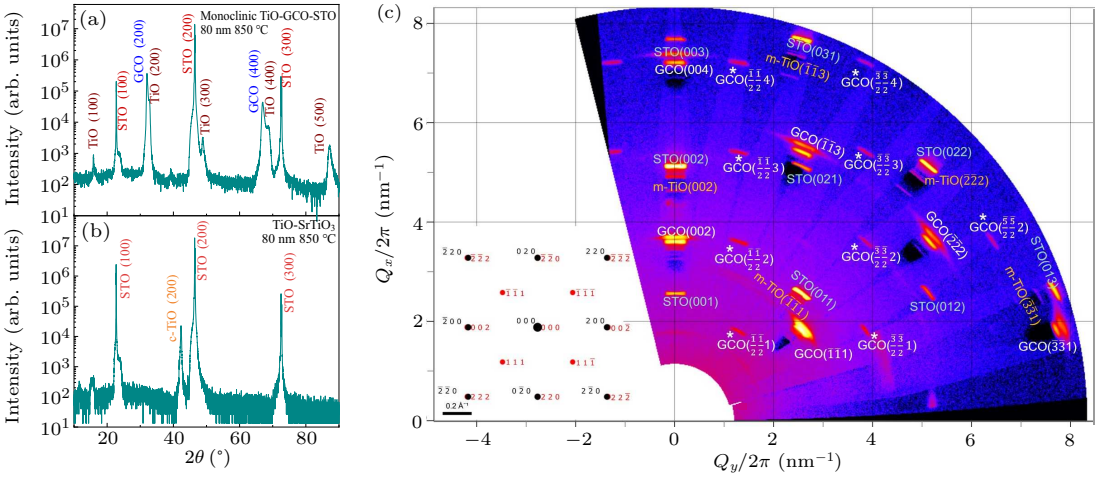


Fig. 2. (a), (b) Out-of-plane XRD θ–2θ scan spectra for TiO film grown on (a) $SrTiO_3$(001) substrate with GCO(001) film intermediate buffer layer and (b) $SrTiO_3$(001) substrate. Two titanium monoxide films were grown under exactly the same conditions which are marked in the figures. (c) Reciprocal space mapping (RSM) of m-TiO(001)/GCO(002)/STO(001) taken along the [100] STO substrate direction. Besides the diffraction spots of $SrTiO_3$ substrate and GCO buffer layer, monoclinic TiO diffraction spots and oxygen vacancy-induced superlattice in GCO can also be distinguished in RSM. Inset shows the simulated diffraction pattern of c-TiO (black) in [001] direction and m-TiO (red) in $[1\bar{1}1]$ direction.

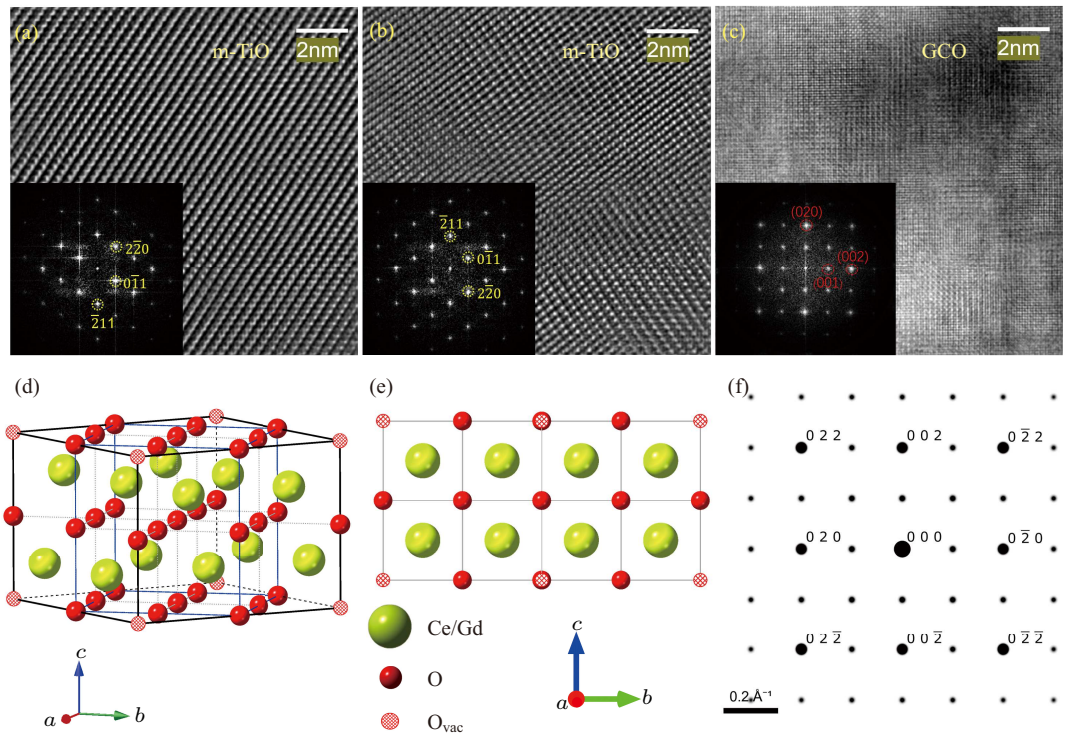


Fig. 3. (a), (b) HRTEM images of monoclinic TiO (m-TiO) film taken along the (a) $[\bar{1}\bar{1}\bar{1}]$ direction and (b) [111] direction belong to the same zone axis. (c) HRTEM image of GCO buffer layer viewed along the [100] direction. Corresponding fast Fourier transform (FFT) inserted. (d) Crystal structure model of GCO supercell with oxygen vacancies located at all eight vertices. The original GCO unit cell is marked by blue lines, and oxygen vacancies are represented by red circles with grid lines. (e), (f) Projected crystal structure and simulated electron diffraction pattern along the [100] direction. The simulated diffraction pattern in (f) shows an exact match with the diffraction pattern in (c).

3.2. Structural characterization of the superlattice in the GCO buffer layer

As mentioned above, the peaks marked with asterisks in the RSM measurements cannot be explained by the expected structural phases. Considering the presence of oxygen ion channels induced by oxygen vacancies in the GCO film,[33] along with the regular positioning of these peaks, we propose the formation of a long-range ordered superstructure within

the GCO intermediate layer, resulting from the reorganization of the oxygen sublattice. This hypothesis is supported by the observation of fractional-order GCO diffraction peaks, which are characteristic of oxygen vacancy superlattices. This interpretation was further confirmed through HRTEM measurements.

As shown in Fig. 3(c), the HRTEM image of the GCO buffer layer reveals the superlattice structure, and the corresponding FFT pattern displays additional diffraction spots. All diffraction spots are indexed to the cubic GCO structure with lattice parameters of $a = 5.42$ Å. Combining this information with the RSM data, we reconstructed this superstructure, and the modulation vector was determined to be $q = 1/2(110)$. The reconstructed superstructure, which incorporates oxygen vacancies, is illustrated in Fig. 3(d). The oxygen vacancies are positioned at the eight vertex sites of the newly formed superstructure unit cell. Specifically, along the [110] direction, an oxygen vacancy occurs every three oxygen atoms, while in the [001] direction, an oxygen vacancy appears at every oxygen atom. Figure 3(e) presents a side view along the [100] direction, providing a clearer visualization of the oxygen vacancy distribution outside the original unit cell. We also performed an electron diffraction simulation for this direction. The simulated diffraction spots along the [100] direction (Fig. 3(f)) match the experimental results well (see the inset of Fig. 3(c)). Additionally, the simulated diffraction pattern along the [110] direction (see supplementary materials, Fig. S2) also aligns with the RSM data. These findings confirm the formation of an oxygen-vacancy-ordered superstructure within the GCO buffer layer. In contrast to prior studies where oxygen vacancies in GCO were considered disordered,[29,30,33] our results indicate a more ordered configuration. The extra peaks marked with asterisks can also be explained by this superstructure.

3.3. Transport measurements of titanium monoxide films

As shown in Fig. 4(a), electrical transport measurements of the m-TiO film reveal superconducting transitions with an onset critical temperature (T_c^{onset}) at 5 K and a zero-resistance state (T_c^0) at 4.4 K. Meanwhile, a characteristic resistivity kink near 120 K, similar to observations in cubic TiO[15] and Ti_4O_7 films,[18] indicates the occurrence of charge localization, potentially due to polaron formation.[34–36] The overall transport behavior is highly similar to that of reported c-TiO and TiO films grown on LSAT substrates (see supplementary materials, Fig. S1). However, the superconducting transition temperature is lower than the 6 K observed for TiO films grown on LSAT substrates, as well as the 7.4 K reported in the literature. Figure 4(b) presents complementary magnetization measurements, which show the emergence of the Meissner state at approximately 4.3 K in both zero-field-cooled (ZFC) and field-cooled (FC) modes, under a 20 Oe magnetic field applied parallel to the film surface. This is in good agreement with the transport-derived T_c^0 in Fig. 4(a), further confirming the superconductivity of the m-TiO film.

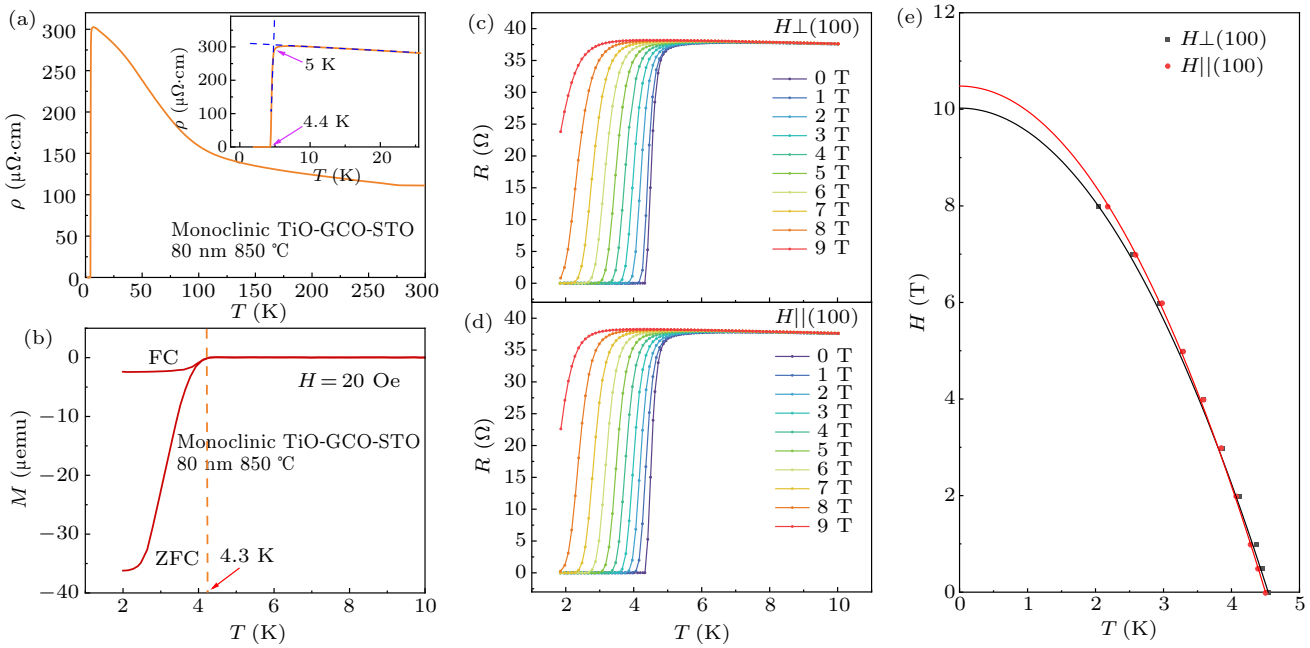


Fig. 4. (a) Temperature dependence of electrical resistivity of the superconducting m-TiO film. Inset shows the magnified resistivity–temperature curve of superconducting m-TiO film, and arrows indicate the point of resistivity transition. (b) Temperature dependence of magnetization of the m-TiO film. During the measurement, an external field of 20 Oe was applied. Moreover, the orange dotted line accompanied with the red arrow indicates that the temperature corresponding to zero resistance is approximately 4.3 K. (c), (d) Temperature dependence of the resistance of the monoclinic TiO film under various magnetic fields from 0 T to 9 T perpendicular (c) and parallel (d) to the film. (e) Temperature-dependent upper critical field $H_{c2}(T)$ for both magnetic field orientations. Solid squares and dots represent experimental data derived from panels (c) and (d) using the 90% normal-state resistivity criterion, with solid curves showing fitting results.

The superconducting properties of m-TiO thin films were further investigated through magnetotransport measurements. Figure 4(c) and 4(d) present the magnetotransport characteristics of the monoclinic TiO film under perpendicular (c) and parallel (d) magnetic field configurations from 0 T to 9 T. The superconducting state exhibits systematic suppression with increasing field magnitude in both orientations, accompanied by a progressive reduction in critical transition temperature. The superconducting response shows minimal field-orientation anisotropy, consistent with c-TiO[15] and Mg:Ti_9O_{10}.[19] This could be attributed to the fact that the film thickness ($\sim$ 80 nm) is significantly greater than its superconducting coherence length (calculated to be $\sim$ 5 nm) and the three-dimensional crystal structure of the titanium monoxide film. Figure 4(e) delineates the temperature-dependent upper critical field ($H_{c2}(T)$) derived using the 90% normal-state resistivity criterion for both field configurations of perpendicular and parallel to the film surface. The experimental data can be well fitted by the relation

$$H_{c2}(T) = H_{c2}(0)\left[1-\left(\frac{T}{T_c}\right)^2\right], \tag{1}$$

where $H_{c2}(0)$ is the upper critical field at absolute zero temperature. The value of the zero-temperature upper critical field $H_{c2}(0)$ can be extrapolated to 10.0 T and 10.5 T in the two cases: perpendicular and parallel to the film, which are smaller than the values of 13.6 T and 13.7 T in the cubic TiO film. [15] Correspondingly, the Ginzburg–Landau superconducting coherence lengths,

$$\xi = \left(\frac{\hbar}{2e}\cdot\frac{1}{2\pi H_{c2}}\right)^{1/2}, \tag{2}$$

at absolute zero temperature are estimated to be about 5.74 nm and 5.60 nm for $H\perp(100)$ and $H\parallel(100)$, respectively. In summary, from the perspective of transport, there are obvious similarities among titanium oxide films with different structures. This phenomenon also highlights the importance of conducting research that distinguishes them from a structural perspective.

Furthermore, we investigated the effect of growth temperature on transport properties while maintaining the monoclinic crystal structure. As shown in Fig. 5(a), XRD patterns of m-TiO films grown at four different temperatures confirm the structural integrity of the monoclinic phase. Corresponding temperature-dependent resistivity curves in Fig. 5(b) reveal diverse behaviors — including strong insulating, weak insulating, superconducting, and pre-superconducting characteristics. Comparable phenomena have also been reported in oxygen-pressure-modulated growth of titanium oxide thin films. For samples exhibiting superconductivity or strong insulating behavior, a distinct resistivity anomaly near 130 K (definition provided in supplementary materials, Fig. S3) is observed. This semiconductor-to-insulator transition is a hallmark feature of all superconducting titanium oxide thin films reported, and some experimental evidence suggests that it may be associated with a first-order phase transition.[15,17–19] In contrast, no clear resistivity kink is observed in the sample grown at the highest temperature. This behavior is reminiscent of molecular beam epitaxy (MBE)-grown c-TiO films in the literature, which also exhibit a superconducting transition temperature of only $\sim$ 0.5 K.[16]

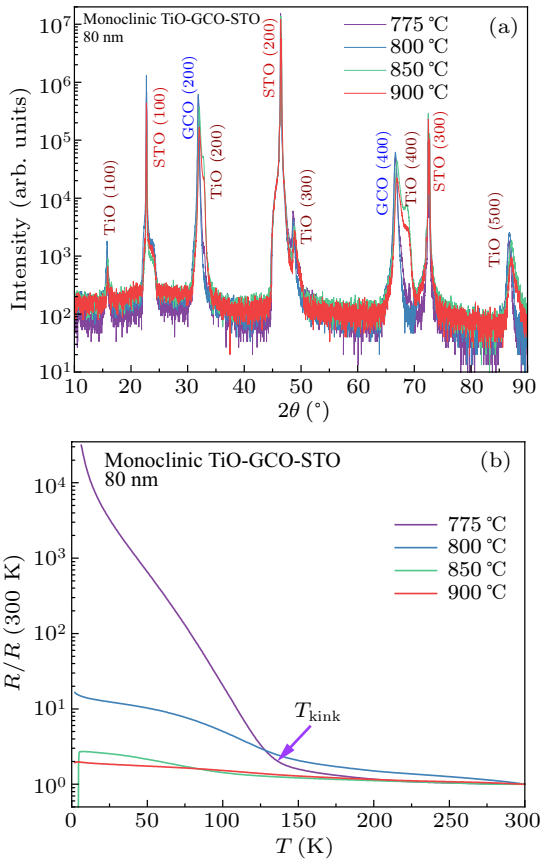


Fig. 5. (a), (b) Out-of-plane θ–2θ XRD scans and normalized resistance as a function of temperature curves of m-TiO thin films at four growth temperatures (775/800/850/900 °C, ascending; denoted by purple/blue/green/red lines, respectively). All other growth parameters remain identical (see Section 2), and XRD peak positions of m-TiO show a slight high-angle shift with increasing growth temperature. All four samples retain the m-TiO phase structure yet exhibit distinctly divergent transport behaviors. The arrow marks the temperature of resistivity anomaly for the sample exhibiting strong insulating behavior, and the definition is presented in the supplementary materials, Fig. S3.

4. Discussion

Previous studies on titanium oxide compounds have largely focused on the identification of thin films with diverse crystal structures, often accompanied by emergent superconductivity. Despite different space groups, these phases show similar transport properties — a key issue in this system, likely stemming from intrinsic structural similarities. When titanium oxide films are grown on MgO substrates, variations in the Ti:O ratio and film thickness can result in the formation of

c-TiO, corundum-type Ti_2O_3, or γ-Ti_3O_5.[20] Our structural characterizations of TiO films grown on Al_2O_3 substrates further demonstrate that with a fixed Ti:O stoichiometry during growth, multiphase coexistence still occurs across different regions of the film.

These findings highlight two key points: first, the critical importance of comprehensive structural characterization in this field; and second, the possibility that many titanium oxide phases share structural motifs. We suggest that these various structures may originate from the cubic phase, evolving through systematic vacancy ordering. However, this intrinsic tendency toward multi-phase coexistence hinders the fabrication of single-phase films, which is crucial for studying their intrinsic properties. We demonstrate that this challenge can be effectively addressed through appropriate substrate selection. Specifically, we achieved a pure monoclinic TiO phase by growing the film on a GCO buffer layer. Notably, wide-range RSM and HRTEM measurements reveal that the lattice mismatch strain between m-TiO and the GCO buffer layer is only 0.36%, substantially lower than the mismatch on LSAT (6.1%) and Al_2O_3 (3.9%) substrates. This indicates that epitaxial strain plays a critical role in directing phase-selective growth in titanium oxide thin films and offers a valuable guideline for future synthesis strategies.

Phenomenologically, it appears that both excessively strong and excessively weak resistivity anomalies are detrimental to superconductivity, consistent with our earlier observations in single-phase Ti_9O_{10} film grown on $MgAl_2O_4$ substrates. These results are generally attributed to polaronic effects. Beyond the titanium oxide family, polaron-induced transport anomalies have been widely reported in other transition metal oxides, and polaron formation is often believed to be closely linked to the mechanism of superconducting pairing.[37–41]

Among all samples, the film with the strongest insulating behavior exhibits the most pronounced resistivity anomaly. We propose that charge transport in this sample is dominated by polarons. To further explore this, we fitted the resistivity data above and below the anomaly temperature using the small polaron hopping (SPH) model and the variable range hopping (VRH) model, respectively (see supplementary materials, Fig. S4). The fitting results support a transport mechanism consistent with polaron hopping: at higher temperatures, polarons hop between neighboring localized states via the SPH mechanism; as temperature decreases, reduced thermal energy necessitates longer-distance hopping, consistent with the VRH mechanism. These results underscore the critical role of polaron transport in the m-TiO system.

As discussed above, we have uncovered the intergrowth feature of titanium oxide thin films grown on conventional substrates, revealing the structural similarity among multiple phases. By employing the GCO buffer layer, we successfully obtained single-phase m-TiO thin films, which allows us to measure their intrinsic transport properties. A superconducting transition temperature of 5 K is confirmed in this system, and fitting results demonstrate that the physical behavior is closely associated with polarons.

Finally, during the growth process, we identified a novel superstructure within the GCO buffer layer. This superstructure likely arises from kinetically driven oxygen vacancy ordering, facilitated by interfacial strain and ionic mobility gradients during heteroepitaxial growth. The formation of oxygen vacancies is known to endow oxide materials with unique physicochemical properties, and oxygen vacancy engineering has received growing attention. Oxygen vacancies can be engineered via several distinct strategies, including the application of external electric fields reported recently and the conventional thermal treatment approach, and in materials such as CeO_2, ordered oxygen vacancies significantly enhance catalytic performance in H_2-related reactions.[42,43] The newly observed superstructure in GCO deepens understanding of oxygen vacancy ordering in CeO_2 systems and offers new insight for designing ordered vacancy structures in functional oxides.

5. Conclusion

We successfully synthesized a superconducting monoclinic TiO thin film epitaxially grown on $SrTiO_3$ substrates utilizing GCO as an intermediate buffer layer, which presents the highest T_c of 5 K. The expanding body of research on superconducting titanium oxide thin films highlights persistent knowledge gaps in identifying commonalities between different compositions. The emergence of the superconducting monoclinic phase provides an important reference for clarifying the similarities and differences among titanium oxides and their transformation trends. An analysis of the transport behavior in the monoclinic phase also helps to understand the key role played by polarons in this system. On the other hand, detailed structural characterization revealed the emergence of an oxygen vacancy-mediated superstructure within the GCO interlayer during heteroepitaxial growth. This ordered oxygen redistribution phenomenon establishes an experimental framework for probing vacancy self-organization mechanisms during thin-film synthesis.

Acknowledgements

This work was supported by the National Natural Science Foundation of China (Grant Nos. 12488201, 12274390 and 12304035), the Anhui Initiative in Quantum Information Technologies (Grant No. AHY160000), the Innovation Program for Quantum Science and Technology (Grant No. 2021ZD0302802), the National Key R&D Program of

China (Grant No. 2022YFA1602600), the Basic Research Program of the Chinese Academy of Sciences Based on Major Scientific Infrastructures (Grant No. JZHKYPT-2021-08).

References

[1] Haeni J H, Irvin P, Chang W, Uecker R, Reiche P, Li Y L, Choudhury S, Tian W, Hawley M E, Craigo B, Tagantsev A K, Pan X Q, Streiffer S K, Chen L Q, Kirchoefer S W, Levy J and Schlom D G 2004 *Nature* **430** 758

[2] Chen Z H, Luo Z L, Huang C W, Qi Y J, Yang P, You L, Hu C S, Wu T, Wang J L, Gao C, Sritharan T and Chen L 2011 *Adv. Funct. Mater.* **21** 133

[3] Kim J, Sekiya T, Miyokawa N, Watanabe N, Kimoto K, Ide K, Toda Y, Ueda S, Ohashi N, Hiramatsu H, Hosono H and Kamiya T 2017 *NPG Asia Mater.* **9** e359

[4] Tokura Y, Takagi H and Uchida S 1989 *Nature* **337** 345

[5] Loktev V M 1996 *Low Temp. Phys.* **22** 1

[6] Rao C N R and Raveau B 1989 *Acc. Chem. Res.* **22** 106

[7] Li D F, Lee K, Wang B Y, Osada M, Crossley S, Lee H R, Cui Y, Hikita Y and Hwang H Y 2019 *Nature* **572** 624

[8] Sun H L, Huo M W, Hu X W, Li J Y, Liu Z J, Han Y F, Tang L Y, Mao Z Q, Yang P T, Wang B S, Cheng J G, Yao D X, Zhang G M and Wang M 2023 *Nature* **621** 493

[9] Ko E K, Yu Y J, Liu Y D, Bhatt L, Li J R, Thampy V, Kuo C T, Wang B Y, Lee Y H, Lee K, Lee J S, Goodge B H, Muller D A and Hwang H Y 2024 *Nature* **638** 935

[10] Wang J, Li Y Y, Deng L, Wei N N, Weng Y K, Dong S, Qi D P, Qiu J, Chen X D and Wu T 2016 *Adv. Mater.* **29** 1603730

[11] Marcelis E J, ten Elshof J E and Morales-Masis M 2024 *Adv. Opt. Mater.* **12** 2401423

[12] Yurddaskal M, Dikici T, Yildirim S, Yurddaskal M, Toparli M and Celik E 2015 *J. Alloys Compd.* **651** 59

[13] Shakir S, Rehman H M A, Yunus K, Iwamoto M and Periasamy V 2018 *J. Alloys Compd.* **737** 740

[14] Banus M D 1968 *Mater. Res. Bull.* **3** 723

[15] Zhang C, Hao F X, Gao G Y, Liu X, Ma C, Lin Y W, Yin Y W and Li X G 2016 *npj Quantum Mater.* **2** 16006

[16] Li F M, Zou Y T, Han M G, Foyevtsova K, Shin H, Lee S J, Liu C, Shin K, Albright S D, Sutarto R, He F Z, Davidson B A, Walker F J, Ahn C H, Zhu Y M, Cheng Z G, Elfimov I, Sawatzky G A and Zou K 2021 *Sci. Adv.* **7** eabd4248

[17] Li Y Y, Weng Y K, Zhang J J, Ding J F, Zhu Y H, Wang Q X, Yang Y, Cheng Y C, Zhang Q, Li P, Lin J D, Chen W, Han Y, Zhang X X, Chen L, Chen X, Chen J S, Dong S, Chen X H and Wu T 2018 *NPG Asia Mater.* **10** 522

[18] Yoshimatsu K, Sakata O and Ohtomo A 2017 *Sci. Rep.* **7** 12544

[19] Zhuang N, Hu W, Zhang Q H, Zhang Y M, Xiong P Y, Li Q, Yuan J, Chen Q H, Zhu B Y, Zhang H, Dong X L, Gu L and Jin K 2022 *Phys. Rev B* **105** 214511

[20] Ozbek Y, Brooks C, Zhang X, Al-Tawhid A, Stoica V A, Zhang Z and Kumah D P 2022 *Phys. Rev. Mater.* **6** 064805

[21] Srivastava A, Rotella H, Saha S, Pal B, Kalon G, Mathew S, Motapothula M, Dykas M, Yang P, Okunishi E, Sarma D D and Venkatesan T 2015 *APL Mater.* **3** 026101

[22] Reichel F, Jeurgens L P H, Richter G, van Aken P A and Mittemeijer E J 2007 *Acta Materialia* **55** 6027

[23] Hou Y Q, Zhuang D M, Zhang G, Zhao M and Wu M S 2003 *Appl. Surf. Sci.* **218** 98

[24] Zheng R Y, Gao X S, Zhou Z H and Wang J 2007 *J. Appl Phys.* **101** 054104

[25] Venables J A, Spiller G D T and Hanbücken M 1984 *Rep. Prog. Phys.* **47** 399

[26] Youm D and Lee S 1993 *IEEE Trans. Appl. Supercond.* **3** 1065

[27] Xu D, Liu L F, Wang Y, Zhu S P, Zhu P and Li Y J 2012 *J. Supercond. Nov. Magn.* **25** 197

[28] Liu L F, Li Y J, Liu H R, Song X K, Hong D, Wang Y, Xu D and Zhu S P 2011 *Proc. SPIE.* **7995** 799527

[29] Lei B, Liu S H, Ma D H, Zhuo W Z, Wang W X, Wu C Q, Ge B H, Ying J J, Xiang Z J, Wu T, Wang Z Y and Chen X H 2023 *Phys. Rev. Mater.* **7** 044002

[30] Lei B, Ma D H, Liu S H, Sun Z L, Shi M Z, Zhuo W Z, Yu F H, Gu G, Wang Z Y and Chen X H 2022 *Natl. Sci. Rev.* **9** nwac089

[31] Liu Z Y, Huang E W, Orozco I, Liao W J, Palomino R M, Rui N, Duchon T, Nemsak S, Grinter D C, Mahapatra M, Liu P, Rodriguez J A and Senanayake S D 2005 *Science* **368** 513

[32] Khivantsev K, Pham H, Engelhard M H, Aleksandrov H A, Kovarik L, Bowden M, Li X S, Tian J, Koleva I Z, Song I, Hu W, Wei X, Sun Y, Tran P, Graham T R, Jiang D, Dean D P, Breckner C J, Miller J T, Vayssilov G N, Szanyi J, Datye A and Wang Y 2025 *Nature* **640** 947

[33] Tsoga A, Naoumidis A and Stover D 2000 *Solid State Ionics* **135** 403

[34] Marezio M, McWhan D B, Dernier P D and Remeika J P 1972 *Phys. Rev. Lett.* **28** 1390

[35] Tonogai T, Takagi H, Murayama C and Mori N 1998 *Rev High Pressure Sci. Technol.* **7** 453

[36] Soma T, Kobayashi T, Yoshimatsu K and Ohtomo A 2021 *J. Phys. Soc. Jpn.* **90** 023705

[37] Chatterjee S and Das I 2023 *J. Alloys. Compd.* **952** 170011

[38] Khan M H, Pal S and Bose E 2015 *Phys. Scr.* **90** 035803

[39] Yamada Y, Hino O, Nohdo S, Kanao R, Inami T and Katano S 1996 *Phys. Rev. Lett.* **77** 904

[40] Franchini C, Reticcioli M, Setvin M and Diebold U 2021 *Nat. Rev. Mater.* **6** 560

[41] Chaudhary P, Nuwal A, Tiwari S C, Paliwal R K and Kakani S L 2013 *Int. J. Supercond.* **2013** 581025

[42] Chen K X, Yuan X Y, Tian Z B, Zou M C, Yuan Y F, Chen Z L, Zhang Q H, Zhang Y Y, Jin X, Wu T P, Shahbazian-Yassar R and Liu G H 2025 *Nat. Mater.* **24** 835

[43] Esch F, Fabris S, Zhou L, Montini T, Africh C, Fornasiero P, Comelli G and Rosei R 2005 *Science* **309** 752